B-8.4 Research on the tropospheric ozone distribution by using a tropospheric chemical transport model

Contact person Seiji Sugata
Department of Atmospheric Environment
National Institute for Environmental Studies
Onogawa 16-2, Tsukuba, Ibaraki 305, Japan
Tel. +81-298-51-2457 Fax +81-298-50-4732
E-mail: sugatas@nies.go.jp

Total Budget of FY1996-FY1998 8,998,000 Yen (FY1998; 2,932,000 Yen)

Key Words tropospheric Ozone, numerical model, deposition

1. Introduction

In this study, the transport and production of ozone in east Asia during the springtime are studied using a regional-scale atmospheric chemistry model. Specifically, the behavior of ozone during the period of May 1-15, 1987, is studied. The relative importance of transport and chemistry on the distribution of ozone is evaluated.

2. Model Description

The production and transport of ozone in east Asia was investigated by use of the Sulfur Transport Eulerian Model (STEM II) regional-scale model. The STEM-II model is a three-dimensional (3-D), Eulerian numerical model which accounts for the transport, chemical transformation, and deposition of atmospheric pollutants. The model has been used quite extensively for scientific studies and policy evaluations in the eastern United States and the Pacific Rim. The current 3-D version of the model is based on the chemical merchanism of *Lurmann et al.* [1986] and *Atkinson et al.* [1989] and modified to include low NO_x conditions and explicit treatment of isoprene. A total of 84 chemical species and 178 gas-phase reactions were included. The 84 species were further divided into 56 long-lived species that were transported and 28 short-lived species such as free radical species which followed the pseudo steady state approximation. The numerical integration of the chemistry was based on a semi-implicit euler method as described by *Carmichael et al.* [1991]. The complete mechanisms with lists of species and reactions in the model are described in detail by *Carmichael et al.* [1986, 1991].

The study domain includes all of Japan, North and South Korea, Taiwan, most of China, and parts of Russia and Mongolia. Each grid box is 1°x1°. This region has dramatic variations of topography, land type, and mixtures of industrial/urban centers and agricultural/rural regions. The interactions between continental and marine influences play a prominent role in determining the effects of pollutant production and transport in this region. The vertical domain covered from the surface to 10 km with an unequal vertical resolution consisting of more layers in the boundary layer and fewer in the middle troposphere.

2.1 Emissions

NO_x emissions for the region are available from several sources including *Fujita et al.*, [1992] and *Akimoto and Narita* [1994]. In this study, NO_x emissions from fossil fuel

combustion were taken from *Akomoto and Narita* [1994]. The largest emissions of NO_x occur in China. However, the emission intensity varies significantly from region to region. For example, the highest emission intensities are found around the main industrial and urban centers such as Tokyo, Seoul, and Shanghai.

The SO_2 anthropogenic emissions were taken from the Central Research Institute of Electric Power Industry (CREIPI) 1987 inventory [Fujita et al., 1991, 1992]. Japan's emission control technology has led to rather low SO_2 emissions, while in contrast, China has the largest SO_2 emission. The emission characteristics vary dramatically from country to country. For example, the SO_2/NO_x ratio is ~5 in China, less than 1 in Japan, and ~1 in Korea.

Anthropogenic hydrocarbon emissions are taken from *Piccot et al.*'s [1992] 10° x 10° global inventory of volatile organic compound emissions. Seven emission categories including formaldehyde, other aldehydes, paraffins, olefins, aromatics, and other aromatics, and marginally reactive compounds are given in this inventory. Corresponding molecular weights were assigned, and the emission values were partitioned into the model's categories of hydrocarbon emissions. The 10° x 10° inventory was interpolated to the model grid by using the distribution of anthropogenic NO_x . These initial nonmethane hydrocarbon (NMHC) emissions are highly uncertain. They were checked by comparing calculated concentrations with observed values at sites in southern Japan. The model-predicted values were found to be systematically lower than the observations, by factors ranging from 3 to 5, depending on the species. The NMHC emissions were adjusted by major category (and uniformly within the study domain) to better match the modeled and observed NMHC values. These results are discussed in more detail by *Uno et al.* [1997].

2.2 Meteorological Data

The three-dimensional meteorological fields needed by the model were obtained from European Center for Medium-Range Weather Forecasts (ECMWF) analyzed winds. This data set provides the horizontal wind speeds in both the zonal and meridional directions and the vertical values at designated atmospheric pressure intervals. The vertical wind fields were recalculated from the given horizontal data using the divergence theorem in order to avoid mass balance inconsistencies that arise when interpolating the wind velocities from the original pressure grid to our vertical grid system. These data are available every 12 hours and are interpolated to provide hourly fields. Other meteorological data used in the simulation were temperature, pressure, relative humidity, and geopotential fields.

2.3. Initial Conditions and Boundary Conditions

The initial conditions were chosen to reflect the Asian situation. Recent measurements were used whenever possible [*Akimoto et al.*, 1993; *Uno et al.*, 1997]. Most of the concentration values were chosen at the lower end of their range so as to allow the emissions and chemical reactions to "taken them up" to their "actual" values during the 2-day initialization period. The boundary condition for the four horizontal surfaces and the upper vertical domain were set equal to the initial conditions.

The horizontal distribution of ozone was set to imitate the naturally occurring increase in the ozone values from the lower to the middle latitudes. Two vertical distributions of ozone were used in different simulations. In one case the initial distribution was prescribed and had higher ozone values in the upper part of the model domain. In case the north and south boundaries for ozone (in ppb) at 0.2, 2, 4, and 10 km were 40 and 15; 55 and 25; 75 and 45;

and 95 and 80, respectively. Ozone concentrations above 10 km were assumed to be 100 ppb, so that when inflow conditions occurred at the top boundary, descending air coming into the model domain had ozone levels of 100 ppb.

In the second case of simulations the initial vertical distribution of ozone, as well as the value of ozone at the top of the modeling domain under in-flow conditions, were scaled to potential vorticity (PV). To calibrate this relationship in east Asia, potential vorticities calculated from ECMWF data were regressed with ozonesonde data at Kagoshima, Tateno, and Sapporo, Japan, for the April and May periods of 1984 through 1991. These three locations span a latitude range from ~30 ° N to 45 ° N, respectively. The observed ozone was regressed against the interpolated potential vorticity at the same location and point in time, using the data below 10 km (the height of upper boundary). The strongest correlation and largest slope were found at the northernmost point (Sapporo, with $r^2 = 0.8$, slope equal to ~76 ppb/10^{-6} km^2 kg^{-1}s^{-1}), and the weakest was found at the southernmost location (Kagoshima, with $r^2 = 0.4$, slope equal to 23ppb/10^{-6} km^2 kg^{-1} s^{-1}). These slope values are somewhat lower than the scaling factors found when the analysis is done using data in the lower 25 km, where values of 50-100 ppb/(10^{-6} km^2 kg^{-1} s^{-1}) are typical. Sensitivity studies were performed using different scaling factors raging from 20 to 35, and these results are presented later in this paper.

2.4. Simulation Procedure and Synoptic conditions

The simulated period was May 1-15, 1987. The staring time was 0000 UT on May 1, i.e., 0900 JST; the transport time step was 15 min, and the gas-phase chemical reactions were calculated every 60 s. Input files were read in at the available intervals, while output file of the major gas-phase long-lived species and radical species concentrations were generated every hour. To investigate the relative roles of in situ photochemical processes and downward transport of ozone-rich air from the upper troposphere, a series of simulations were conducted. Simulations included cases with all the transport, chemistry, and deposition processes.

The period of study is typical of springtime conditions in east Asia. The dominant feature was strong continental outflow associated with traveling cold fronts. The flow fields used the modeling analysis are shown in Figure 1. Wind vectors and geopotential heights at 850 and 300 hPa are shown along with the locations of the major high and low pressure systems. The shading in the 300-hPa plots indicate regions of negative (downward) vectical velocities.

During the first few days in May, strong conditional outflow occurred from northeast China and Korea associated with the intense low-pressure system shown clearly, for example, in the plots for May 4. The region of strong continental outflow during this period was limited to latitudes higher than ~40 ° N. Below 40 ° N a high-pressure system was located over eastern China. The situation over the next few days dominated by a slow moving high-pressure system that passed over Japan from eastern China to the central Pacific Ocean during the period from May 5 to May 14. A cut off low formed on the Japan Sea on May 8 and moved to the east over the next several days. The plots for May 9 show clearly the strong continental outflow from northeast China and the transport around the high-pressure system located over Japan. The air mass was divided into two parts as it traveled around Japan, with the lower part transported to the south in association with the cut off low. Strong downward transport was associated with the cut off low as shown in the 300-hPa plots. The high pressure region was pushed to the east after May 10, as the next cold front passed over Japan (see, for example May 12 and 14).

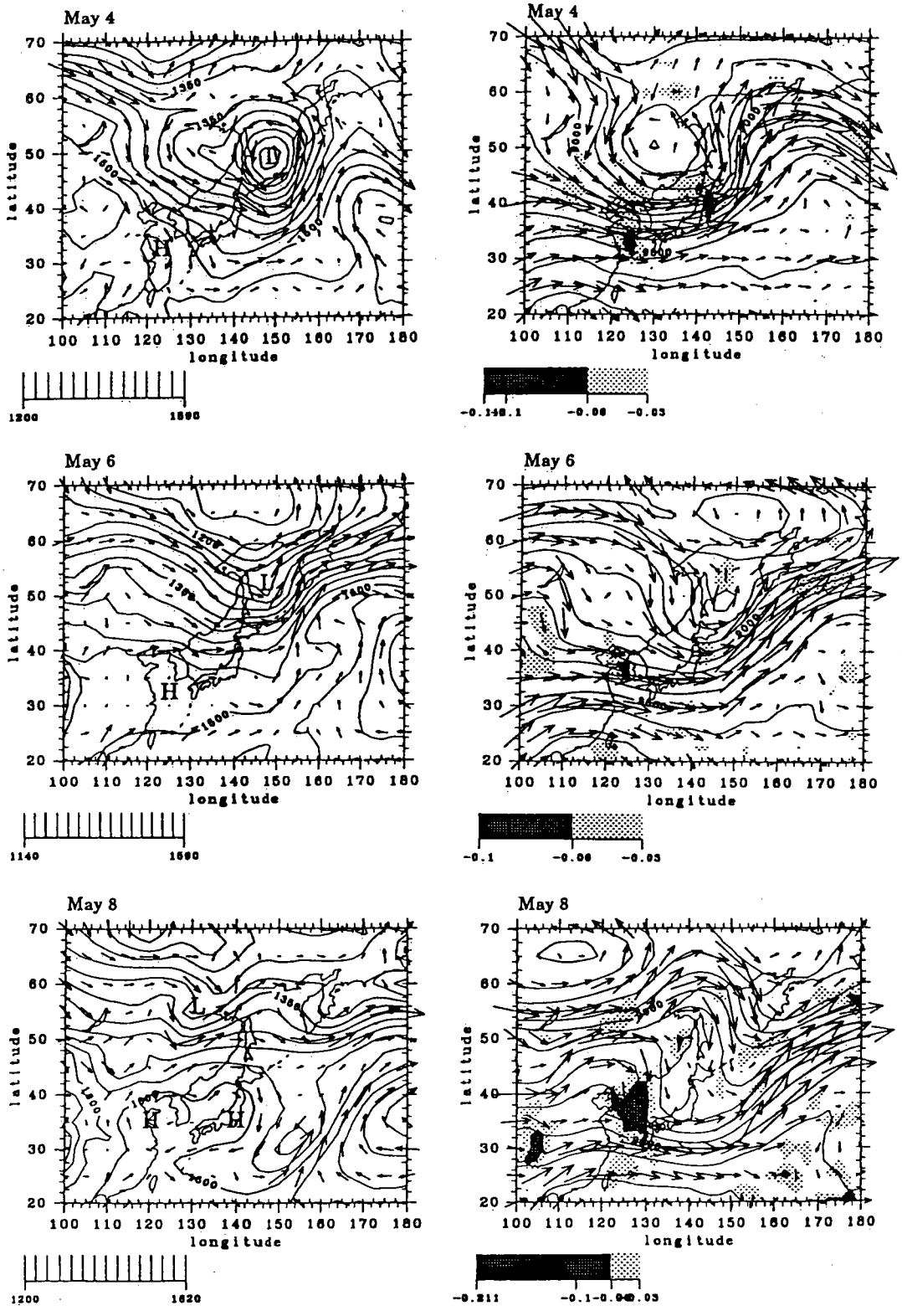

Figure 1. Flow fields on May 4, 6, 8, 9, 10, and 12, 1987 at (left) 850 hPa and (right) 300 hPa. The contours on the 850-hPa plots indicate the geopotential height (in meters). The shaded areas on the 300-hPa surfaces represent regions of negative (downward) velocities (m/s), with the lighter shading indicating downward velocities between -0.03 and -0.06 m/s and the darker shading indicating velocities greater than -0.06 m/s.

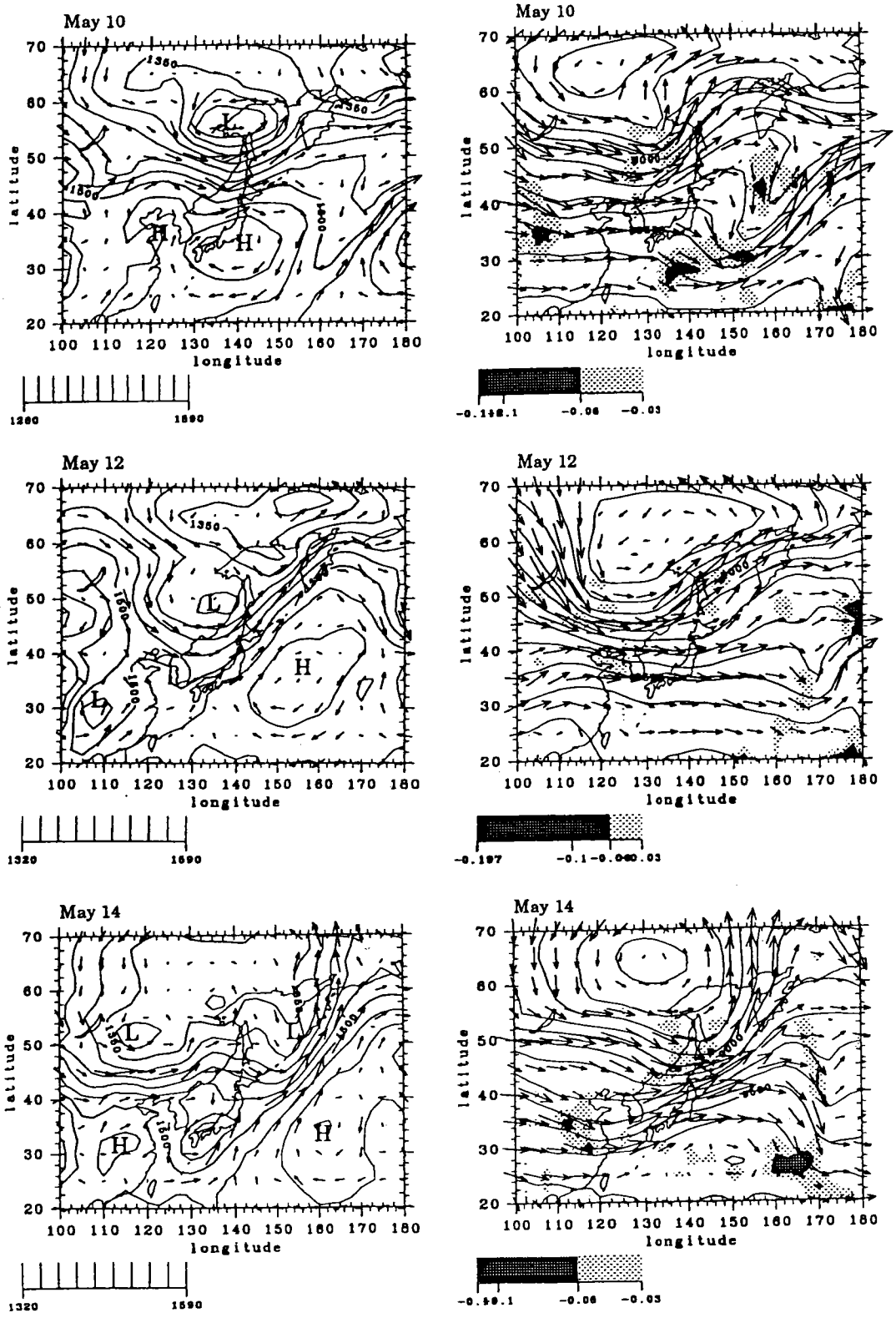

Figure 1. (continued)

3. Results and Discussion

3.1. Near Surface Ozone Distribution

Shown in Figure 2 are the large-scale ozone features at 1500 LT and a height of 1 km on May 4, 6, 8, 9, 10, and 12, calculated for the simulation with full chemistry, transport, and removal, and with the ozone initial distribution and top boundary condition set using PV

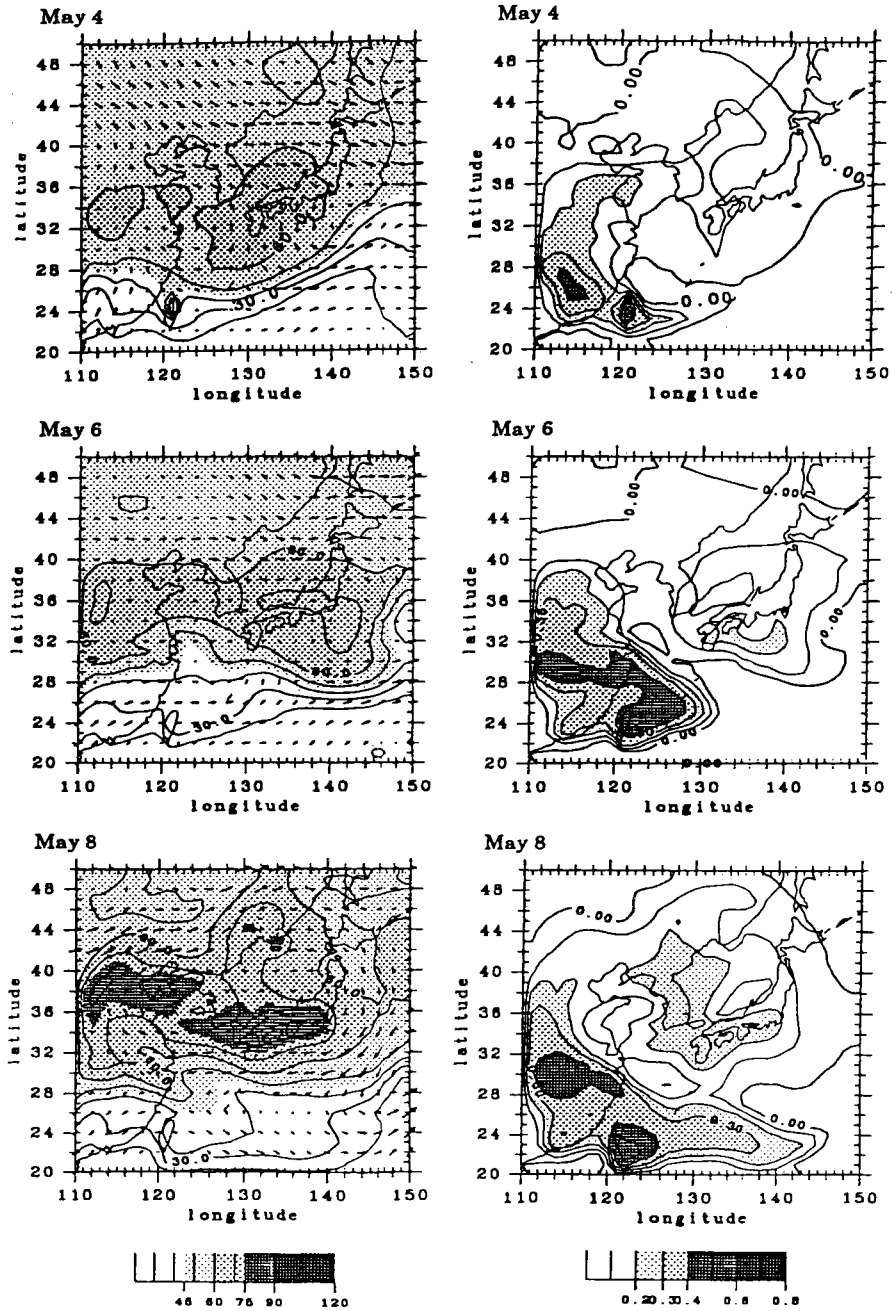

Figure 2. (left) Calculated ozone (ppb) at 1500 LT for the full chemistry, transport, and deposition simulation (CHEM_PV35) at 1 km. The ozone distribution is shown by both shading and contour intervals, with the darker shading indicating ozone in excess of 90 ppb. Also shown are the horizontal wind vectors at the same time and height. (right) The fractional changes in ozone due to photochemical processes (i.e., (CHEM_PV35 - TRANS_PV35)/TRANS_PV35). Positive values indicate an increase in ozone levels due to chemical processes.

with a scaling factor of 35 (CHEM_PV35). The high wind speeds and sinking motions behind the cold front resulted in a large region of high ozone (greater than 60 ppb) centered over Japan on May 4. From May 6 to 8, elevated ozone levels were found in association with the high-pressure systems. For example, on May 8, there were two high-pressure cells, one to the west of Korea and the other centered over the western tip of Japan (see Figure 1). Between these high-pressure systems was a region of strong subsidence, which resulted in high ozone (greater than 60 ppb) in the lower layers. High ozone levels were also found over Beijing on

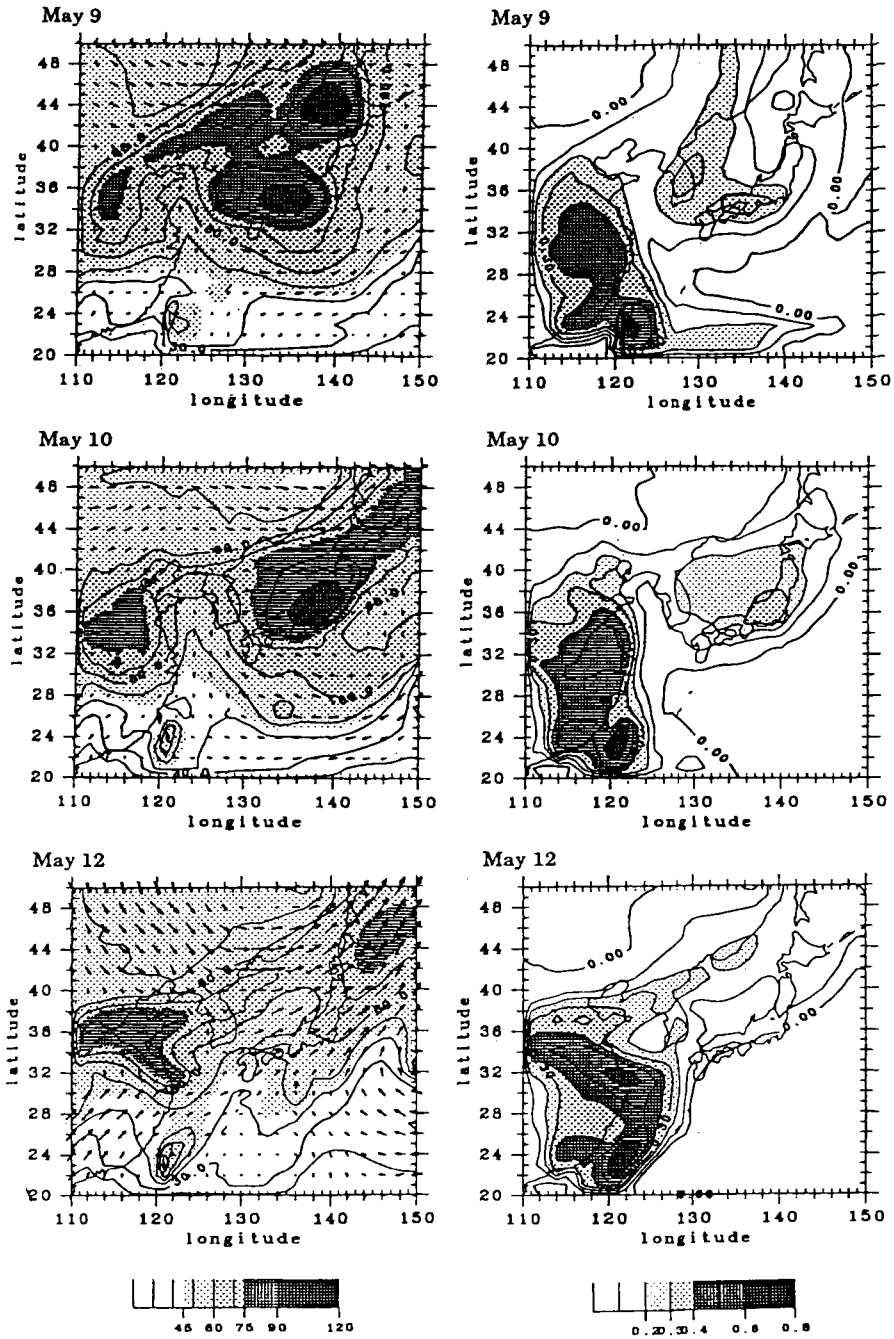

Figure 2. (continued)

the backside of the high-pressure system. The movement of these ozone-rich pockets is clearly shown in the plots for May 8-12, where the high ozone air masses are transported in a clockwise manner within the high pressure system and out the northeast boundary of the domain in the frontal zone between the backside of the high and the approaching low-pressure system. Another persistent feature is a region of elevated ozone centered over the high anthropogenic emission area of eastern China. This area was under the influence of high pressure and light winds throughout the simulation period. The ozone produced in this region was subsequently transported around the high-pressure system and then off the continent in the latitude band of 35 ° -40 ° N.

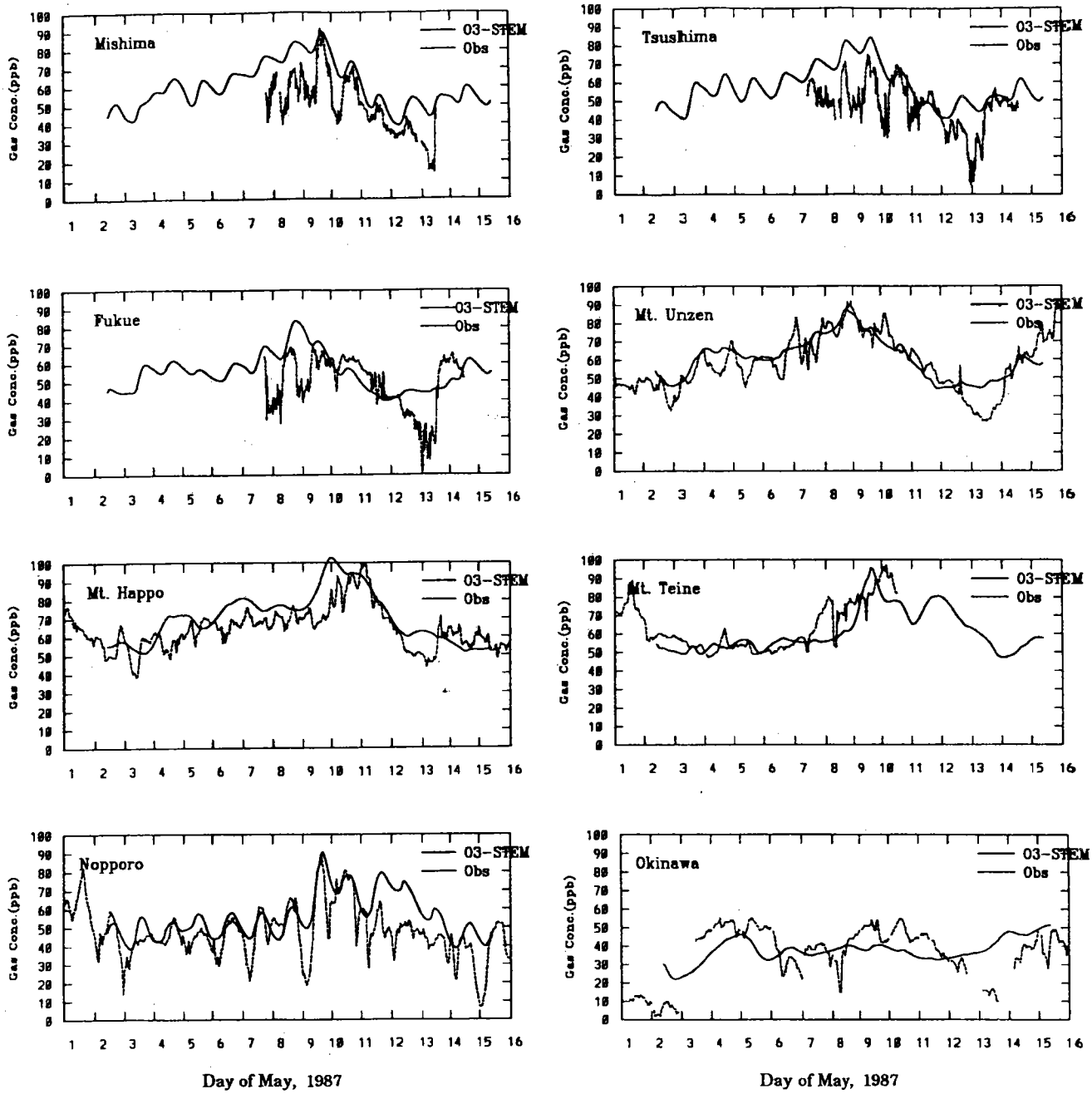

Figure 3. Comparison between predicted ozone for the full chemistry, transport and removal simulation (CHEM_PV35), and observed surface ozone at eight locations in Japan.

The predicted ozone fields are compared with surface ozone measurements from a network of stations in Japan in Figure 3. The locations of the measurement sites range from island sites (e.g., Okinawa and Tsushima) to mountain sites (e.g., Mount Happo and Mount Teine, etc.) and span the latitude range of ~25 ° N-~45 ° N. In most cases the model accurately predicts the surface ozone levels, especially the synoptic-scale features. For example, the daily variations in surface ozone at Mt Happo are accurately captured. The cold front passed through this region around May 3, and as the high-pressure system formed over Japan the ozone levels increased, reaching a peak value of ~100 ppb on May 10. By May 14 the high-pressure system had moved to the east of Japan, and Mt Happo was on the backside of the high and under the influence of the marine air with much lower ozone. The magnitude

of the peak ozone levels and the timing of the low ozone concentrations were accurately captured, while the timing of the peak was off by ~1 day and the minimum values were overpredicted by ~10 ppb at this site. The movement of the ozone maximum across Japan associated with the movement of the high-pressure system is clearly seen in both the observations and the predictions. For example, the ozone maximum of ~90 ppb occurred at Mt Unzen on May 9 and at Mt Happo around May 11.

The diurnal variation in ozone at the mountain sites is much less than that at the island sites. While the model captures these features, the diurnal variation in model is too weak, especially at the island sites. This is not surprising, given the coarse resolution of the grid (horizontal 1 ° and vertical ~0.3 km) and the meteorological input data (interpolated from 6-hour values), and the highly parameterized eddy diffusivity profiles used in the calculation.

3.2. Vertical Ozone Distribution

The analysis of the near-surface ozone time series indicates that the horizontal aspects of the meteorological fields are reasonably well captured in the analyzed fields used in the simulation. The vertical aspects of the flow are critical, especially when attempting to quantify the contributions from transport versus chemical process. During this time period an intense field campaign took place in southern Japan, and rawinsonde mesurements were taken at the Japan Meteorological Agency upper air station at Kagoshima (located near Mount Unzen (31.4 ° N, 130.5 ° E)) every 12 hours. The observed vertical distribution of water vapor and winds in the lowest 10 km are shown in Figure 4. Also shown are the relative humidity profiles used in the model. The vertical profiles of water vapor used in the calculations are very similar to the observed values. Both the observed and analyzed water vapor fields show the passage of the cold front on May 2, with high water vapor concentrations extending into the middle troposphere, followed by sinking air (as shown in Figure 1) with low relative humidity, associated with continental outflow. High pressure settled over the region beginning on May 6 and caused relative humidities to increase throughout the troposphere. A strong subsidence accompanied the passage of the second cold front on May 8 (shown clearly in the 300-hPa plot in Figure 1), and air low in water vapor was transported from the upper troposphere to within a few kilometers of the surface. This was followed by the influx of marine air on the backside of the strong high-pressure system that slowly moved to the east during May 11-14.

The calculated ozone distribution at Mount Unzen is also shown figure 4. The strong downward transport of ozone-rich air from the upper troposphere toward the surface around May 8, associated with the strong subsidence zone, is clearly shown. Air masses with ozone levels in excess of 100 ppb were transported down to ~2 km above the surface. This cold, low relative humidity air is indicative of the upper troposphere.

In general, the regions of high ozone correspond closely with the regions of downward motions. The downward transport of ozone occurs in conjunction with the traveling cyclones (lows) associated with these spring weather systems. One mechanism leading to elevated ozone in the troposphere is the intrusion of lower stratospheric air into the troposphere associated with the wobbling of the jet stream. Under this mechanism the highest convergence of ozone is expected to occur under the jet stream along the boundary of the troughs.

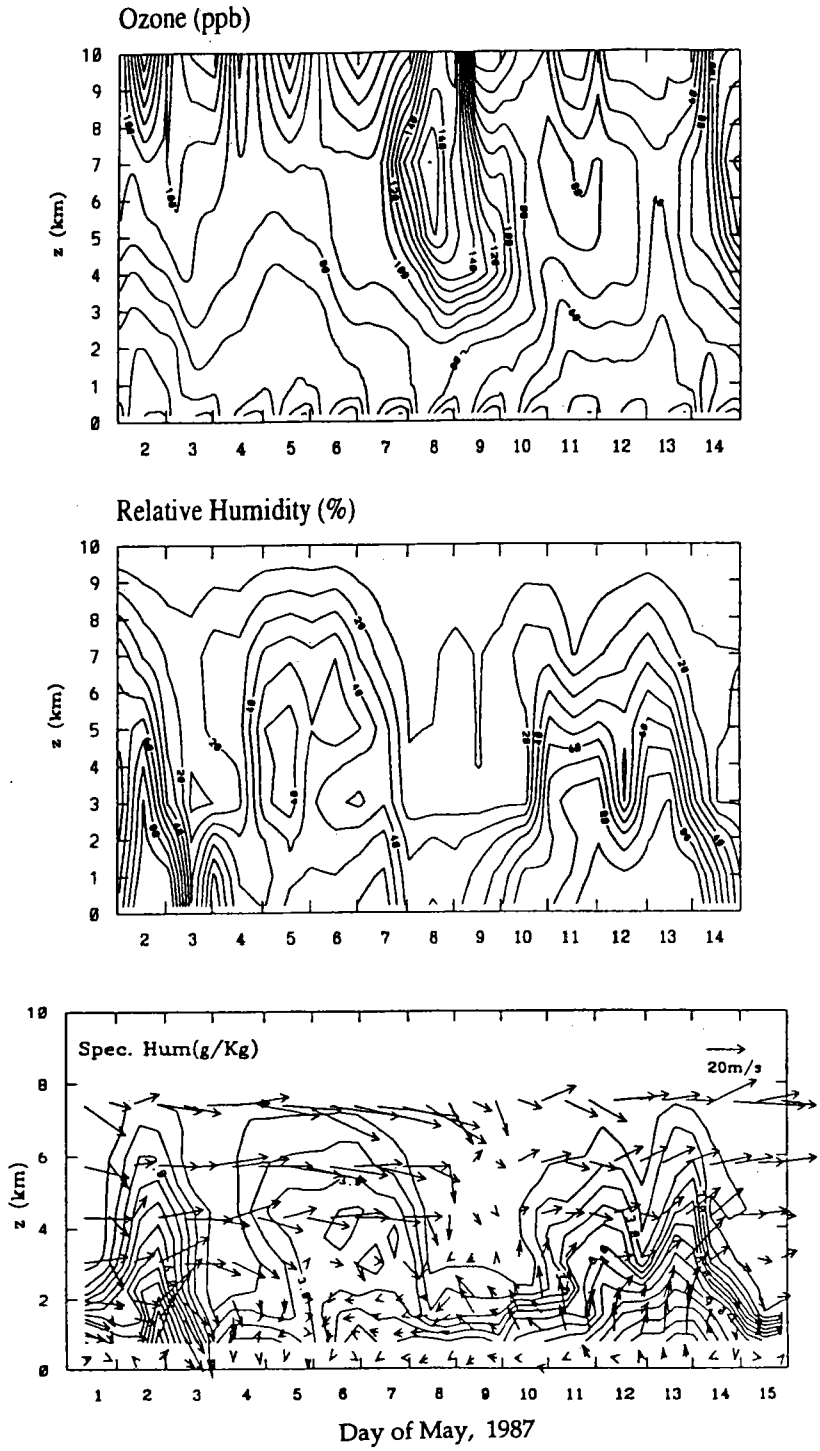

Figure 4. The vertical distributions of ozone and water vapor at Mt Unzen. The top panel displays the calculated vertical distribution of ozone as a function of time for the full chemistry, transport, and removal simulation (CHEM_PV35). The middle panel shows the modeled relative humidity distribution The bottom panel shows the observed vertical distributions of specific humidity and wind vectors at Mt Unzen.

4. Summary

The transport and production of ozone in east Asia during the springtime was investigated using a regional-scale atmospheric chemistry model. Specifically, the behavior of

ozone during the period of May 1-15, 1987, was studied. High ozone levels were observed during this period in association with the passage of cold fronts. The relative importance of transport and chemistry on the distribution of ozone was evaluated by performing simulations with and without chemical processes. The model predicted ozone values were compared with surface observations in Japan and were found to accurately capture many of the important observed features. The best model results were obtained with an upper surface boundary condition which scaled O_3 to potential vorticity.

The transport processes associated with the passage of the cold front were found to play a critical role in determining the spatial distribution of ozone. Strong downward fluxes of ozone from the upper troposphere toward the surface occurred behind the cold fronts and below the upper level low-pressure center. High ozone levels were transported to 1-2 km above the surface by the high-pressure systems which trail the cold fronts. These transport processes were able to account for many of the synoptic-scale features in the observed ozone fields at Happo, Japan. The region above 30° -35° N was most heavily impacted by downward transport of ozone.

The photochemical production of ozone was found to be important in the regions over the precursor source regions and in the continental outflow zones. Calculated production efficiencies for ozone were found to be similar to those observed and calculated over North America. The regions of strong photochemistry were largely restricted to the lowest 3 km of the atmosphere. However, in regions of convective activity the chemical production zones reach the middle troposphere. These results indicate that ozone in the lower troposphere in this region can be strongly influenced by both continental outflow of precursors and by the downward transport of ozone-rich air which occurs frequently in conjunction with strong continental outflow episodes.

References

Akimoto, H., and H. Narita, Distribution of SO_2, NO_x, and CO_2 emissions from fuel combustion and industrial activities in Asia, *Atmos. Environ.*, **28**, 213-255, 1994.

Atkinson, R.J., W.A. Matthews, P.A. Newman, and R.A. Plumb, Evidence of the mid-latitude impact of Antarctic ozone depletion, *Nature*, **340**, 290-294, 1989.

Carmichael, G.R., L.K. Peters, and T. Kitada, A second generation model for regional-scale transport/chemistry/deposition, *Atmos. Environ.*, **20**, 173-188,1986.

Carmichael, G.R., L.K. Peters, and R.D. Saylor, The STEM-II regional scale acid deposition and photochemical oxidant model, I, An overview of model development and applications, *Atmos. Environ.*, **25A**, 2077-2090, 1991.

Fujita, S., Y. Ichikawa, R. Kawaratani, and Y. Tonooka, Preliminary inventory of sulfur dioxide emissions in east Asia, *Atmos. Environ.*, **25A**, 1409-1411, 1991.

Fujita, S., et al., *Acid deposition in Japan*, Report, 90 pp., Cent. Res. Inst. of Elec. Power Ind., Tokyo, Japan, 1992.

Lurmann F.W., A.C. Lloyd, and R. Atkinson, A chemical mechanism for use in long-range transport/acid deposition computer modeling, *J. Geophys. Res.*, **91**, 10905-10936, 1986.

Piccot, S.D., J.J. Watson, and J.W. Jones, A global inventory of volatile organic compound emssions from anthropogenic sources, *J. Geophys. Res.*, **97**, 9897-9912, 1992.

Uno, I., S. Wakamatsu, H. Ueda, K.Murano, S. Sakamaki, H. Kurita, H. Satsumabayshi, and S. Horai, Behavior of secondary pollutants and volcanic SO_2 over Kyushu during a spring high pressure system, *J. Jpn Soc. Atmos. Environ.*, **32**, 404-424, 1997.